Long-Term Dynamic Thermal Ratings of Underground Cables Integrating Soil Dynamics and Climate Projections

Sergio Daniel Montana Salas, Andrea Michiorri

Long-Term Dynamic Thermal Ratings of Underground Cables Integrating Soil Dynamics and Climate Projections

Montana Sergio, Michiorri Andrea

February 12, 2024

Abstract

Underground Cables capacity is influenced by thermal properties, particularly the interplay between dynamics of the physical properties and the surrounding soil's heat dissipation capabilities. This paper introduces a new approach to quantifying the long-term effect of climate conditions and soil dynamics on underground cable capacity that leverages machine learning techniques to estimate soil temperature and moisture in the depth range of 0.8 to 1.2 meters. The research extends its focus to assess the impact of climate change using various representative concentration pathways across 52 European stations. The main strength of this model lies in its ability to offer detailed estimations by capturing the relationships among different types of soils. The results show that the quasi Dynamic Thermal Rating methodology produces an average increase in ratings of 7.1%. In addition, it has the potential to further widen the disparity between winter and summer seasons, with an increase of up to 8.1%. Regarding climate impacts, there are moderate reductions over the medium-term emissions horizon, with an average reduction of 0.27% to 0.63%.

Keywords: Underground Cables, Climate change, Dynamic Thermal Rating, Transmission.

1 Introduction

The rising adoption of Underground Cables (UGC), driven by expanding renewable generation plants [1], poses a challenge for a warmer, energy-demanding future [2]. Meteorological factors and climate changes significantly affect UGC capacity, mainly reliant on the surrounding soil's effectiveness in dissipating joule losses. This heat transfer mechanism, impacted by moisture and soil thermal resistivity, holds the potential for up to 50% capacity reduction [3], which cannot be captured using the traditional approach of energy utilities for capacity limits. In this context, large-scale soil factor measurements play a crucial. However, only historical high-resolution models combining data with observations have emerged in the last decade [4, 5], with a gap in long-term projections for burial depths between 1 and 5 meters. This underscores the significance of our research in understanding the complexities of climate-induced changes and their implications for the transmission sector over the long term.

To cope with the effects of temperature rise and optimize cable current carrying capacity, Dynamic Thermal Rating (DTR) [6–13] is actively proposed as a technology that aims to identify the real-time current carrying capacity to optimize asset utilization, reduce congestion and improve efficiency as a function of environmental conditions such as ambient and soil temperature. It is crucial to emphasize that the primary objective, as presented in [14], positions DTR as a strategic tool for system operators. It aids in accurately and reliably determining current rating limits, thereby alleviating constraints based on thermal considerations.

As the temperature is the primary variable in the DTR, weather or mechanical characteristics can be determined from two methods: i) Real-time measurement equipment, known as direct. Usually performed nowadays for brand new circuits with an embedded optical fiber as described in [15], offering excellent accuracy and precision, but with barriers such as capital costs and non-applicability to already installed networks. ii) Thermal mathematical model based on information from meteorological conditions, with a non-steady state thermal model using historical data or numerical weather predictions [16]. Deployed as a method that increases capacity compared to static thermal power but reduces the risk of overloading.

When this model is applied, meteorological factors and climatic changes have a discernible impact on the DTR ratio [8], as established by well-known international standards such as IEEE Std 1863 [17] and IEC 60287 [18]. This impact is vital in defining the parameters used for rating estimation, described by energy conservation and heat transfer mechanisms [19, 20] of the cable's physical properties and the surrounding soil's heat dissipation capabilities. Notably, the heat balance highlights the challenge of low heat dissipation in

UGC exposed directly to the environment (direct soil buried). Understanding and quantifying these factors is critical to assessing UGC systems' thermal performance and overall efficiency.

A crucial parameter influencing the rating within the soil's thermal properties is the soil thermal resistivity (^{o}Cm/W), highly correlated with the moisture content [17,18,21]. This effect becomes particularly significant when its impact is translated into temperature. In [3], a 50% reduction in the rating is observed when the soil thermal resistivity is three times greater and the ambient temperature increases by 5 ^{o}C. Reinforcing its high dependence and correlation between temperature and humidity of the surrounding soil, among other factors, such as laying depth and physical properties [22].

The utilization of in-situ sensors for measuring soil moisture and temperature at various spatial scales, as discussed in [23, 24], presents an opportunity to comprehend the interrelationship and devise a solution to estimate the intricate interaction in exchange processes between land-atmosphere interactions and soil. Consequently, considerable research efforts have been directed towards this objective over the past few decades. Noteworthy contributions include satellite observations [25], microwave remote sensing, and physically-based models [26], providing spatiotemporal estimations. However, these methods may experience deviations in performance due to complex topography and transient climate conditions [4, 25, 27]. On the other hand, Machine-Learning models (ML) employing remote sensing data have been applied in various research studies [4,28–32] with a broad spectrum of data integration. These models, primarily influenced by climatic conditions and soil taxonomy, including texture and soil type, present a novel alternative that challenges conventional processes. By "learning" the intricate interdependencies between meteorological variables and soil dynamics, they redefine the approach to understanding and modeling these intricate connections.

A limited number of strategies have been developed, incorporating ML in DTR for UGC [33, 34]. As outlined in [35], an approach that involves the development of a day-ahead DTR forecast relies on a Support Vector Regression (SVR) method for soil temperature. However, the physical-statistical model for predicting thermal conductivity, applying a regression model for soil-specific heat, exhibits reduced simulation accuracy across diverse soil types, limiting its general applicability. To analyze the thermal conductivity and cover a wide range of soil texture, bulk density, temperature, and moisture, in the last decades, several estimations models have been proposed [36–41]. In [42], a new empirical model for estimating soil thermal conductivity was developed. For this, a comprehensive evaluation of several approaches was performed and is influenced by many factors such as organic matter, soil texture, and particle composition. Resulting in a performance of R^2 of 0.98, increased simulation accuracy for ten soil types.

As temperature and soil moisture conditions become increasingly common variables in planning and managing the capacity of UGC [8], establishing projections related to the energy transition is a critical step in quantifying and understanding the impacts associated with climate change. To tackle the issues outlined above, the contributions of this paper are:

a) Introduce a probabilistic DTR method aiming to exploit transmission capacity efficiently and minimize the risk of overloading as part of long-term power system planning

c) Assess trends and possible impacts of climate change on UGC in the long term horizon.

The paper is organized as follows: Section 2 illustrates the machine learning process, thermal model, and methodology. Results are described in Section 3, and conclusions are drawn in Section 4.

2 Methodology

2.1 Overview

We develop a model to quantify the long-term effect of climate conditions on UGC capacity, summarized in the block diagram Fig. 1. First, supervised ML models are trained using historical in-situ measurements [43] and meteorological information [5, 44] in module **2.2**. Secondly, meteorological time series data from both historical [43, 45] and machine learning projections are collected in module **2.3**. These data are fed to components' thermal models to calculate the time series for the transmission capacity in modules **2.5**,**2.4**. Subsequently, in the final module **2.6**, a probabilistic approach integrated into DTR is proposed [46, 47] by fitting a probability distribution to the lower tail of the simulations for each month/hour combination and selecting an accepted level of risk tolerance to thermal overload (0.1% in this case).

2.2 Machine Learning Model

This module aims to target soil moisture ($\hat{\psi}$) and temperature ($\hat{\Theta}_s$) data at 0.25°, with a daily resolution in a depth range between 0.8 and 1.2 meters based on hourly-recorded input data. The pre-selection of the features

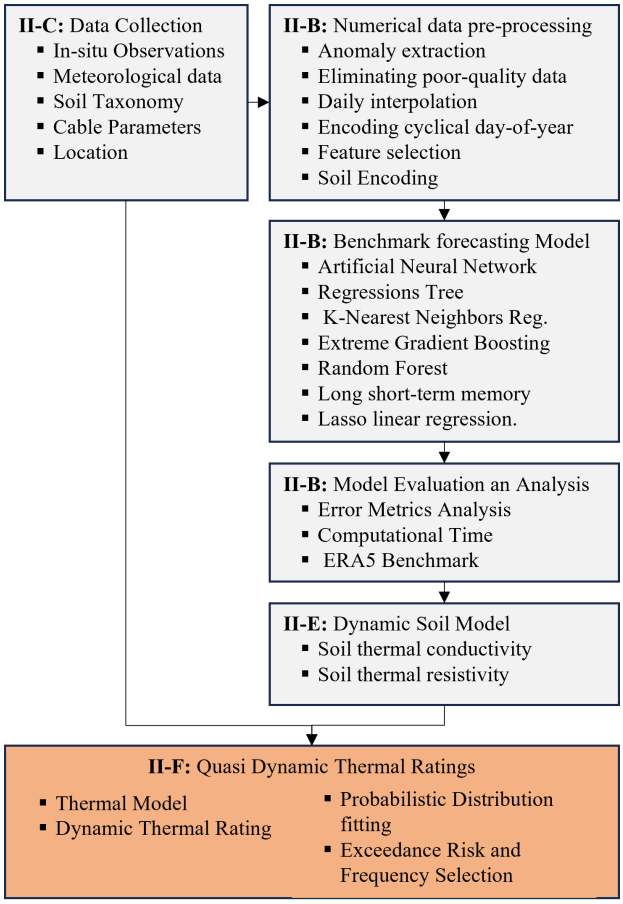

Figure 1: Block scheme of the approach proposed for calculating quasi Dynamic Thermal Ratings in UGC.

was performed under a combination of time series of meteorological data, soil properties, and observations, mainly based on bibliographic analysis [4, 29, 30, 32]. To ensure the spatiality of the system throughout the European region, we rely on the open sources described in the section 2.3.

Due to the problem's complexity, we implemented the following preprocessing and numerical transforms: a) Anomaly extraction. b) Eliminating poor-quality data [48] c) Excluding stations with less than three months of annual information d) Daily interpolation e) Encoding cyclical Day of the Year (t_c) f) Minimum and maximum scaling [49] f) Feature selection conducted to achieve the highest prediction accuracy. g) Finally, to ensure broad operability, each analyzed soil is encoded (S_{code}) by soil texture classification according to [50] and texture represented in Table 1.

In the initial phase, an evaluation of various machine-learning techniques was carried out in order to select the most appropriate for our method. This assessment focused on key error measurement indicators such as Root Mean Squared Error (RMSE) and Mean Absolute Error (MAE), with particular emphasis on the computation time of the predictions. Evaluation metrics are given with the following equations:

$$\mathrm{RMSE}_q = \sqrt{\frac{1}{H}\sum_{i=1}^{H}(y_{q,i} - \hat{y}_{q,i})^2} \tag{1a}$$

$$\mathrm{MAE}_q = \frac{1}{H}\sum_{i=1}^{H}|y_{q,i} - \hat{y}_{q,i}| \tag{1b}$$

In the equations, $\hat{y}_i$ denotes the estimate of humidity and temperature, while y_i represents the observation for the same variables from ISMN stations. The subscript H signifies the projected horizon of the estimation. As described in the previous section, a reduction in UGC ratings is associated with lower humidity and higher temperature. Thus, our analysis focuses on the heightened risk of overloading, the metrics described in equations , are evaluated the lower 20th quantile for humidity and the 80th quantile for temperature, and denoted as q.

Table 1: REVISED USDA SOIL TEXTURE CLASSIFICATION, INDICATING SOIL CODES USED IN THIS STUDY

Texture Class	Sand %	Silt %	Clay %	Code
Sand (S)	> 85	0-15	0-15	5
Loamy Sand (LS)	70-85	0-20	0-15	5
Sandy Loam (SL)	43-70	7-20	0-27	4
Loam (L)	20-40	40-60	7-27	4
Silt Loam (SiL)	0-20	≥ 70	0-27	4
Silt (Si)	0-10	80-90	0-10	4
Sandy Clay Loam (SCL)	20-35	28-50	27-40	3
Clay Loam (CL)	20-35	28-50	27-40	3
Silty Clay Loam (SCLa)	0-20	50-70	27-40	3
Sandy Clay (SC)	0-20	0-28	40-60	2
Silty Clay (SCla)	0-10	50-70	40-60	2
Clay (C)	0-20	0-20	≥ 60	1

The importance of the calculation time is due to the expected regional application of the continental-scale model, highlighting the need for accuracy and efficiency. The techniques evaluated include Artificial Neural Network (ANN) [51], Regressions Tree (RT), K-Nearest Neighbours (k-NN), Extreme Gradient Boosting (XgBoost) [52], Random Forest (RF) [53], Long short-term memory (LSTM), and Lasso linear regression [54].

Considering the soil-inertia nature in the output variables as detailed in [4], this model is supervised-trained with observations lagged by five days. This lag was determined through time series analysis using a partial auto-correlation function (PACF) [55]. The dataset is divided by stations and soil types to train and test the models. The training set is then randomly divided into 70%, with 10% reserved for tuning the model hyper-parameters using techniques from [49, 56]. The remaining 30% serves as a validation set to test the model. To avoid overfitting, N-fold cross-validation is performed by applying the metrics described in (1) by dividing the test dataset into five folds, ensuring all soil types are present in each fold, thus guaranteeing homogeneity of selection.

2.3 Datasets

Quantifying the impact on UGC capacity is conducted by processing data derived from a combination of soil properties and meteorological variables of the interest region, as outlined in Table 2.

Considering 100year climatologists, ECMWF ERA5 and Copernicus climate change service (C3S) datasets provide the historical reanalysis[(a)] [5] and climate projections with a Representative Concentration Pathway (RCP) of 2.6, 4.5, and 8.5[(b)] [45]. The high-grid resolution of 0.25° datasets provides a time series from January 01, 1970, to December 31, 2072. However, climatic projections are linearly interpolated with a time resolution of one day to match the frequency of the In-Situ data.

Observing temporal variations in soil is crucial for estimating soil moisture and temperature behavior and assessing sensitivity to climate change and soil taxonomic properties. This mandates the availability of soil moisture datasets that exhibit superior quality, extended duration, continuity, and consistency. In this study, in situ soil moisture[(d)], taxonomy[(c,d)], and temperature measurements[(d)] sourced from the International Soil Moisture Network [43] and [57] are employed. The dataset involves data from 52 networks, spanning the years 2006 to 2022 and covering depths from 0.05 to 120 m.

2.4 Steady-State Thermal model with Moisture Migration

In line with standard procedures for quantifying the ampacity of buried UGC, a thermo-electric model from [18] is employed. According to this standard, the capacity, with the influence of a dry area formation, is calculated per each day (i) as follows:

$$B = W_d \left[\frac{1}{2} T_1 + n \left(T_2 + T_{3i} + v_i T_{4_i} \right) \right] \tag{2a}$$

$$C = n R_i \left(1 + \lambda_1 + \lambda_2 \right) \left(T_2 + v_i T_{4_i} \right) \tag{2b}$$

$$I_i = \sqrt{\frac{\Delta\Theta_i - B + (v-1)\Delta\Theta_x}{R_i T_1 + n R_i (1+\lambda_1) T_2 + C}} \quad \forall i = 1..H \tag{2c}$$

Table 2: DATASETS AND PARAMETERS

Variable	Units	Process	Source	
Meteorological				
Temp. Air at 2 m (Θ_a)	$^{\circ}C$	2.2	a,b	Dynamic
Total precipitation (P_t)	mm	2.2	a,b	Dynamic
Net surface solar radiation (S_r)	Jm^{-2}	2.2	a,b	Dynamic
u - v - wind at 10 m	ms^{-1}	2.2	a,b	Dynamic
Soil Proprieties				
Silt ($S_{silt_{\%}}$)	%	2.5,2.2	c	Static
Sand ($S_{sand_{\%}}$)	%	2.5,2.2	c	Static
Clay ($S_{clay_{\%}}$)	%	2.5,2.2	c	Static
Organic ($S_{org_{\%}}$)	%	2.5	c	Static
Texture Composition (S_{text})	-	2.2	c	Static
Bulk (S_{bulk})	kgm^{-3}	2.5,2.2	c	Static
Soil Measurements				
Temperature (Θ)	$^{\circ}C$	2.2,2.6	d	Dynamic
Moisture (ψ)	%	2.2,2.5	d	Dynamic

The above equation focuses on the critical temperature of the boundary between the wet and dry zones $\Delta\theta_x$ and the ratio between the thermal resistivities of the dry and wet zones of the back-fill soil v_i. With high dependence on variable factors such as ambient temperature, moisture, and precipitation, the other parameters such as λ_{1-2}, C, R, T_{1-3}, W_d obey the cable construction. These parameters can be determined and calculated according to [3, 18], guide and suggestions.

Where the thermal resistance T_4 of the surrounding medium for a single core cable, lay horizontally, is defined as

$$T_{4_i} = \frac{\rho_{s_i}}{2\pi}\left\{\ln\left(u+\sqrt{u^2-1}\right)+\ln\left(1+\left(\frac{2L}{S_1}\right)^2\right)\right\} \tag{3}$$

Where ρ_{s_i} is the thermal resistivity of soil, S_1 spacial axis distance between cables, u is the ratio of the distance from the surface to the cable axis L, and the external diameter of the cable D_e. Hence, it is imperative to calculate ρ_{s_i}, and the analysis must also incorporate considerations based on the cable environment. In conclusion, the relationship between the buried UGC's capacity and the input parameters can be described as a function of Eq. (4). This relationship holds true for uniform soils, where thermal properties remain constant at each coordinate.

$$I_{DTR_i} = I(\Theta_i, \rho_{s_i}, \psi_i, \text{constant parameters}) \tag{4}$$

2.5 Dynamic Soil Model

Modeling soil moisture and temperature dynamics is an area that has been developed over the last century. Differential equations involving consideration of various factors have been presented, as described in the previous section. A one-dimensional representation of heat flow in a vertical direction (x) is outlined in (5), in which the thermal diffusivity α_s is characterized as a direct relationship between the thermal conductivity (λ_s) and the inverse of the soil density and specific heat capacity.

Our approach will implement the dynamics model addressing the physical properties and processes within soils using machine learning, as described in Section 2. However, a mathematical model correlating soil hydraulic-physical properties with thermal conductivity (λ_s) needs to be established to determine the thermal resistivity of each analyzed soil.

$$\frac{\partial \Theta}{\partial t} = \alpha_s \frac{\partial^2 \Theta}{\partial x^2} \tag{5}$$

To address this, the estimation of soil thermal conductivity, which is the inverse of ρ_s, is conducted following the interrelation proposed in [41,42]. This involves unsaturated soils and incorporates parameters such as λ_{dry}, λ_{sat}, and the Kersten coefficient K_e.

$$\lambda_{s_i} = (\lambda_{sat_i} - \lambda_{dry_i}) K_{e_i} + \lambda_{dry_i} \quad \forall i = 1..H \tag{6a}$$

$$K_{e_i} = \exp\left(\alpha - \psi_i^{-\beta}\right) \tag{6b}$$

Here, α and β represent the shape factors of the volumetric water content (ψ) and thermal conductivity curve, respectively. These factors exhibit linear relationships with particle size distribution ($S_{\%}$) and organic matter content ($S_{org_{\%}}$), as defined below:

$$\alpha = a_1 S_{\text{Sand}_{\%}} + a_2 S_{\text{Silt}_{\%}} + a_3 S_{\text{org}_{\%}} + a_4 \tag{7a}$$

$$\beta = b_1 S_{\text{Clay}_{\%}} + b_2 S_{\text{org}_{\%}} + b_3 \tag{7b}$$

Where, the weighting factors of the physical parameters of the model are as follows

Table 3: WEIGHTING FACTORS FOR THE EMPIRICAL MODEL OF THE SOIL THERMAL CONDUCTIVITY

a_1	a_2	a_3	a_4	b_1	b_2	b_3
0.493	0.86	0.014	0.778	0.736	0.006	0.222

At this point, the thermal conductivity is calculated for each soil using the features described in Table 2. This, in turn, allows us to estimate the v ratio and the thermal resistivity of the soil ρ_s per day.

2.6 Quasi Dynamic Thermal Ratings

Finally, a quasi-dynamic Thermal Ratings (qDTR) is applied to calculate ratings for a long-term horizon, as proposed in [46, 47]. After collecting the time series and parameters described in Sections 2.3 and 2.5, the DTR is calculated using (2),(3). These time series are fitted with a probability distribution described in [58], in the lower tail of the simulations for each month/day combination. An accepted level of tolerance to the risk of thermal overload (0.1% in this case) is then selected.

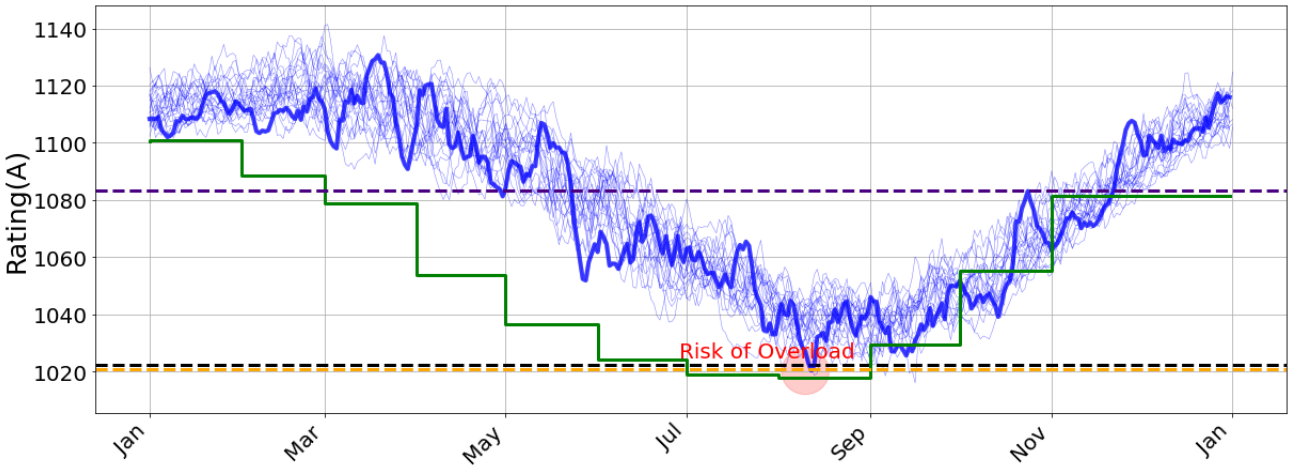

Figure 2: The conceptual illustrations of this proposed method display the DTR calculated throughout a year (2000-2022) for a specific coordinate, represented in blue. The STR_{H} is depicted in black, the monthly qDTR_{H} in green, and the qDTR_{H_s} for the winter and summer seasons in indigo and orange, respectively

This method is conceptually illustrated in Fig. 2. First, the thermal model calculates the maximum capacity-DTR over a 1-year horizon. In contrast plotted as a dash black line, the Static Thermal Rating

(STR_H) applies a fixed value as a constrained capacity limit throughout the year, under-utilizing the UGC and potentially overloading, regardless of changing conditions, with a 0.1% exceedance probability. The $qDTR_H$ is then calculated with the same risk of exceeding over the lower tail values of the DTR across a 50-year time horizon for a monthly/yearly approach, as shown in the central figure. Finally, the $qDTR_{H_s}$ is calculated for winter and summer with the same industry seasonal approach.

3 Results

This study applies qDTR to estimate the maximum allowable currents of UGC using historical (from 1970 to 2022) and future (from 2023 to 2070) weather projections for Europe. The HV cable used in this paper is described in Table 4 obtained from [59] and complemented from [18], with a manufacturer reference A2X(F)K2Y-800RM.

Table 4: UNDERGROUND CABLE PARAMETERS

Parameter	**Default Value**	**Unit/Symbol**
Name	Cable A2X(F)	-
Conductor Material	Aluminium	-
Insulation Type	XLPE	-
Conductor type	Segmental	-
L	1000	mm
ρ_{20}	2.826×10^{-8}	$\Omega \cdot$ m
α_{20}	4.03×10^{-3}	1/K
Θ	90	°C
tan (δ)	1×10^{-3}	-
U_0	72500	V
ε	2.5	-
Frequency	50	Hz
S	400	mm
C	0.295×10^{-9}	F/m
R_0	0.0367×10^{-3}	Ω/m^2
d_c	33	mm
D_e	69	mm

Firstly, to apply qDTR, the data described in 2.3 needs retrieval. For projecting humidity and temperature based on each representative concentration pathway, a machine learning model with a daily step was trained, validated, and selected as outlined in 2.2.

The performance of each model was compared with the ERA-5 data, which were used as a benchmark. Results not shown in this paper indicate that techniques such as KNN and LST, with deviations of $+0.05m^3m^{-3}$ over the observations, increase the computational cost. On the other hand XGBoost [52], as illustrated in (8), and Lasso [54] described in (9), exhibited the most favorable performance for humidity and temperature, in the techniques evaluation process. This was evidenced by achieving the lowest error values among all models, outlined in Table. 5 and 6.

$$\hat{\psi}_i = \sum_{k=1}^{K} f_k(x_i) \tag{8a}$$

$$\mathbf{x_i} = [[w_s, \Theta_a, S_r, t_s]_{i-5:i-1}, S_{\%}, S_{code_{1-5}}] \tag{8b}$$

Where $\mathbf{x_i}$ is the flattened feature vector for the i-th observation

$$\hat{\Theta}_i = \mathbf{x_i} \cdot \hat{\beta}_L \tag{9a}$$

$$\hat{\beta}_L = \arg\min_{\beta} \left\{ \frac{1}{2H} \sum_{i=1}^{H} (\Theta_i - \mathbf{x}_i \cdot \beta)^2 + \lambda \sum_{j=1}^{p} |\beta_j| \right\} \tag{9b}$$

$$\mathbf{x_i} = [[\Theta_a, S_r, t_s]_{i-5:i-1}, S_{\%}, S_{code_{1-5}}] \tag{9c}$$

β is the coefficient vector associated with the features, $\hat{\beta}_L$ is the estimated parameter vector using LASSO and λ is the regularization parameter.

Table 5: MACHINE LEARNING PERFORMANCE - TEMPERATURE AT 80TH PERCENTILE

		Model					
	CV	0	1	2	3	4	ERA
$RMSE_{80}$	0	2.23	2.03	2.29	2.15	2.39	2.72
	1	2.69	2.43	2.73	2.63	2.83	3.64
	2	2.92	4.81	3.19	3.16	3.37	2.76
	3	2.02	1.85	2.25	1.90	2.14	2.90
	4	2.89	3.48	2.60	3.11	2.70	3.56
	Avg.	**2.71**	**3.16**	**2.83**	**2.74**	**2.95**	**3.10**
MAE_{80}	0	2.23	2.03	2.29	2.15	2.39	2.72
	1	2.56	4.61	2.85	2.84	3.06	2.18
	2	1.71	1.55	1.95	1.61	1.87	2.32
	3	2.55	3.14	2.26	2.77	2.38	2.58
	4	2.64	2.96	3.03	2.56	3.41	2.21
	Avg.	**2.34**	**2.86**	**2.48**	**2.39**	**2.62**	**2.40**

Table 6: MACHINE LEARNING PERFORMANCE - MOISTURE AT 20TH PERCENTILE

		Model					
	CV	0	1	2	3	4	ERA
$RMSE_{20}$	0	0.29	0.07	0.13	0.08	0.14	0.22
	1	0.05	0.21	0.08	0.09	0.08	0.15
	2	0.05	0.03	0.10	0.04	0.04	0.09
	3	0.05	0.06	0.06	0.16	0.05	0.07
	4	0.13	0.08	0.11	0.05	0.19	0.24
	Avg.	**0.11**	**0.09**	**0.10**	**0.08**	**0.10**	**0.16**
MAE_{20}	0	0.29	0.06	0.11	0.07	0.13	0.22
	1	0.04	0.21	0.08	0.08	0.07	0.14
	2	0.04	0.03	0.11	0.03	0.04	0.08
	3	0.04	0.05	0.05	0.17	0.04	0.06
	4	0.12	0.07	0.10	0.04	0.19	0.24
	Avg.	**0.11**	**0.08**	**0.09**	**0.08**	**0.09**	**0.15**

The results are derived from diverse station selected through cross-validation, as detailed in Table 7. This table provides information on the various soil codes used. For a graphical representation of the performance across different soil codes, refer to in Fig. 3. At first glance, the XGBoost Moisture model demonstrated lower average error values than the ERA5 model. It is essential to note that MAE has the same units, m^3m^{-3}. With marginally superior performance, the Lasso temperature models denote the robustness of ERA5, establishing themselves as a dependable choice for historical references.

From here, we quantify the climate impact of transmission network capacity for underground cables. The qDTRs are fitted with a probability distribution commonly employed to characterize natural phenomena [58]. Specifically, the power law distribution is applied to the lowest 2% of the calculated ratings for each month/day combination. Across all month/hour combinations, considering an exceedance probability of 0.1%, the results show that the coefficient of determination (r^2) exceeds 0.9.

Table 7: FIVE-FOLD CROSS VALIDATION FOR MOISTURE AND TEST

Description			CV Fold					
ID	Station	Soil Code	1	2	3	4	5	Test
1	SOD140	3						
2	Borda Coll	4						
3	Hupsel	5						
4	Kehrigk	5						
5	Hoal-08	3						
6	Ribera de Sio	4						
7	ITCSM-15b	5						
8	ITCSM-05d	5						
9	ITCSM-06b	3						
10	Camidels Nerets	4						
11	Kuusamo	5						
12	ITCSM-10c	5						
13	Marsh Bubnow	3						
14	San Pietro Capo	4						
15	Voulton	4						
16	Abrahams	5						
17	ITCSM-17c	5						
18	SOD071	3						
19	Falkenberg	4						
20	PoriII	4						
21	ITCSM-14c	5						
22	ITCSM-05c	5						
23	Clot de les Peres II	1						
24	Clot de les Peres I	1						
26	Suizy	1						
27	Serra de CostaAmpla	1						
28	ITCSM-03b	5						
29	Kvarstadseter	5						
30	Pessonada	4						
31	La Cultiada	4						
32	Hoal-07	3						

This procedure is applied to the three projected RCP scenarios, revealing a moderate but noticeable effect of temperature increase according to climate projections, as shown in Fig. 4. Preliminary results suggest that colder temperatures, increased precipitation, and reduced irradiance levels contribute to increased capacity during winter. For instance, in the $\mathrm{qDTR}_{\mathrm{H_w}}$ scenario, the increase may be as high as 8.1%. Additional analysis of this chart reveals a decrease – albeit small – of 0.56% in $\Delta_{\%}\mathbf{(qDTR_{RCP4.5}, qDTR_H)}$ for this specific location. Conversely, a temporal shift in the usual annual temperature cycle is noticeable, with lower capacity observed around September. This phenomenon is attributed to the thermal memory and inertia inherent in buried cabling, causing a time delay in temperature exchange between different layers. The same inertia translates into low daily variability, suggesting that these devices can be effectively analyzed at lower frequencies. This is exemplified by the dashed line, which indicates a monthly ($\mathrm{qDTR}_{\mathrm{H_{month}}}$) analysis approach.

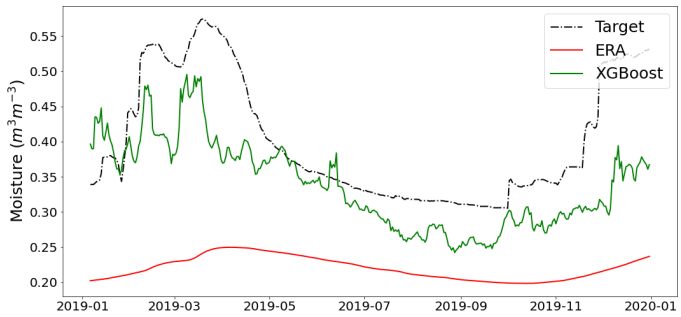

(a)

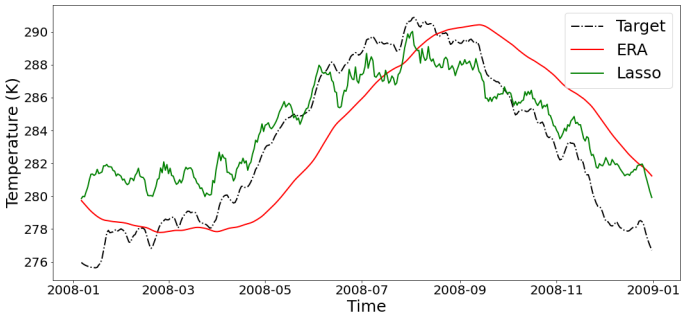

(b)

Figure 3: Daily time series of estimated soil moisture with (a) XGBoost at Soil[5] and (b) LASSO (Green) at Soil[2] compared to ERA data (RED) and Test Values (Black dash)

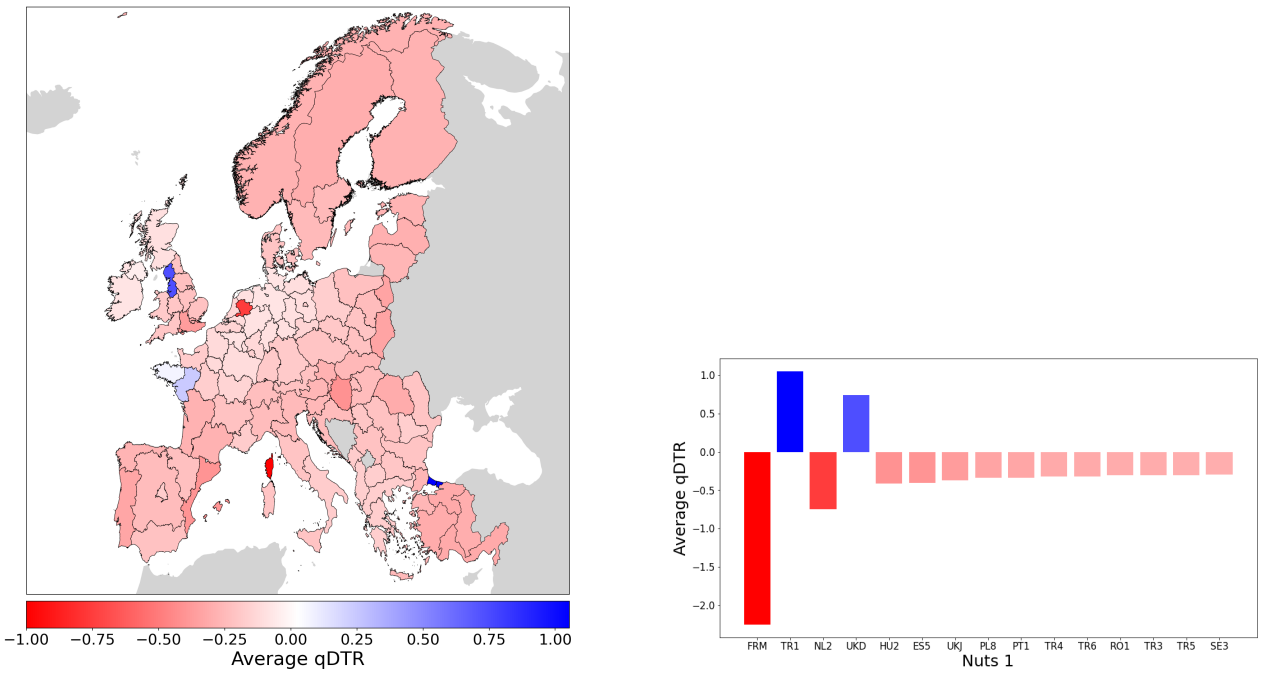

(a) (b)

Figure 5: (a) The calculated delta values between historical $qDTR_H$ and $qDTR_{RCP_{4.5}}$ (b) Ten most representative Nuts 1 regions in Europe

Fig. 5 illustrates the spatial distribution of thermal ratings across NUTS-2 regions in Europe (Nomenclature of Territorial Units for Statistics [60]), highlighting regional differences in the effects of climate change on underground cable capacity. The visualization showcases the spatial variability of $\mathrm{qDTR_H}$ in Europe, with fluctuations of up to 2%. This variability, almost unanimously negative, is influenced by diverse soil types across regions, significantly impacting thermal diffusivity and moisture retention.

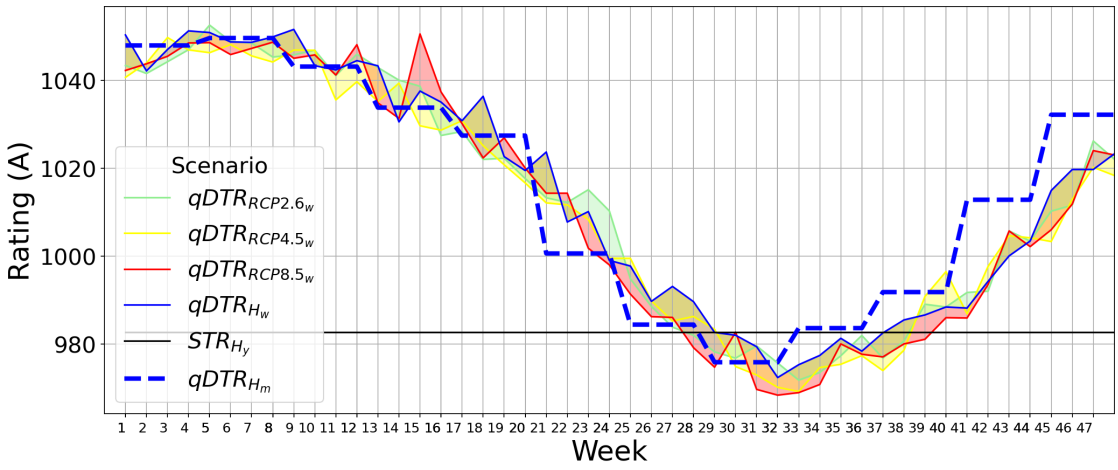

Figure 4: Yearly representation of $qDTR_{week/month}$ for historical $qDTR_H$ values and projections $qDTR_{RCP_{2.6,\ 4.5,\ 8.5}}$ in node located in South Spain, in-dash blue the $qDTR_{H_{month}}$ as a reference

Finally, the same procedure is applied on a country scale, and the results are summarized in Table 8 and geographically represented in Fig. 6. The UGC location retrieved from [61] and described as average, maximum decrease for the qDTRs calculated for the ten lines. It is possible to observe an average reduction in ratings in the order of 0.16%, 0.27%, and 0.33%, respectively, for the 2.6, 4.5, and 8.5 RCP. With maximum peaks in the high emission scenario of 1.38 %

The research investigates the methodology employed in [62], while also offering a broader perspective on additional components.

Table 8: qDTR differences over a fifty-year period for $qDTR_{RCP_{2.6,\ 4.5,\ 8.5}}$ and $qDTR_H$ datasets for 10 UGC in France

Line	Hist	$\Delta_{\%}RCP_{8.5}$		$\Delta_{\%}RCP_{4.5}$		$\Delta_{\%}RCP_{2.6}$	
ID	(A)	Mean	Max	Mean	Max	Mean	Max
1257	1073	-0.44	-1.19	-0.31	-0.88	-0.13	-0.79
8566	1012	-0.42	-0.48	-0.24	-0.09	-0.21	-0.01
5676	1110	-0.36	-0.69	-0.21	-0.59	-0.14	-0.29
8554	941	-0.33	-0.77	-0.42	-0.98	-0.21	-0.37
5808	1002	-0.33	-0.53	-0.39	-0.99	-0.22	-0.23
5792	1006	-0.30	-1.14	-0.13	-0.41	-0.15	0.00
2271	947	-0.30	-1.38	-0.19	-0.91	-0.08	-0.70
8178	1046	-0.27	-1.20	-0.27	-0.60	-0.19	-0.91
8544	1094	-0.27	-0.53	-0.25	-0.43	-0.07	-0.27
5730	1085	-0.23	-0.55	-0.30	-0.40	-0.20	-0.50
Average		-0.33	-0.85	-0.27	-0.63	-0.16	-0.41

4 Conclusions

Through an assessment conducted at a grid resolution, this analysis investigates the impact of climate on transmission network capacity using established thermal models. Employing the Quasi-Dynamic Thermal Rating method to estimate maximum capacity with a low-risk exceedance probability, Our findings highlight moderate reductions in the mid-term emission horizon for underground cables, showing sensitivity to potential climate changes, with a mean reduction from 0.27% to 0.63%. It reflects that the variation caused by the meteorological conditions in the lower risk scenario (0.1%) is reduced at depth buried cables. Conversely, the

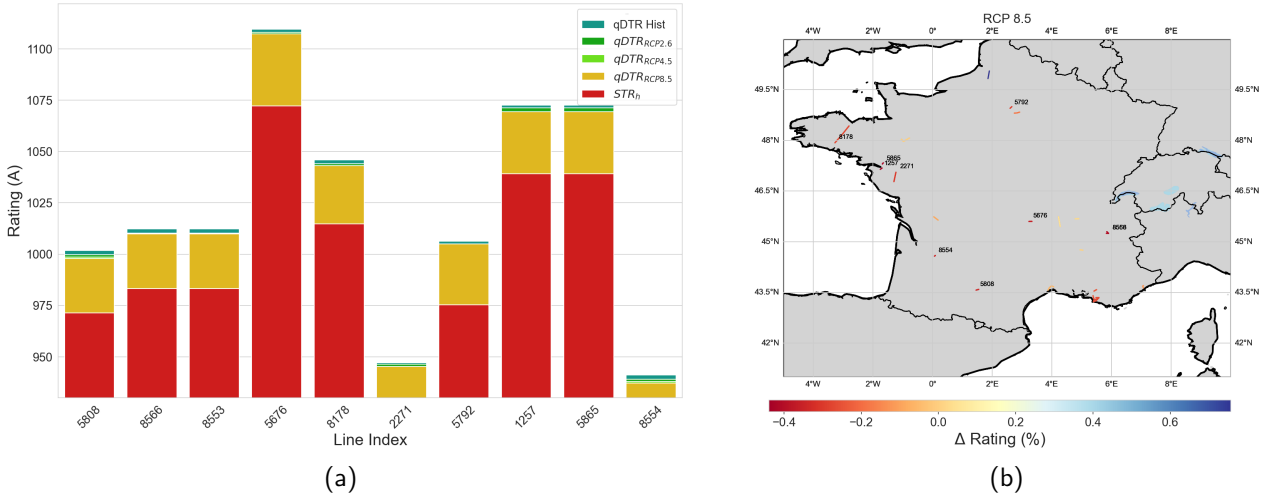

Figure 6: Comparative Analysis: Assessing qDTR variations among historical $qDTR_H$, STR_H, and RCP projections $qDTR_{RCP_{2.6,\ 4.5,\ 8.5}}$ at ten French UGC (b) Regional Analysis: Examining variations in UGL assessments between historical data and $RCP_{8.5}$ projections across France

soil type change could reduce up to 57% of the capacity. In addition, the results reaffirm the previous literature findings showing the heat balance has a memory, i.e., soil moisture anomalies may persist for weeks or even months into the future (monthly rate change less than 5%).

In addition, this paper estimated soil moisture and soil temperature at a depth of 1 meter. The results, obtained through 5-Fold validation, demonstrate mean absolute errors of 0.08 ($\pm$ 0.02) m^3m^{-3} for soil moisture and 2.51 ($\pm$ 0.17) (^oK) for soil temperature. This highlights a better accuracy than the benchmark model and gives more strength to the present study. As part of a future improvement proposal for this module, we suggest integrating additional soil layers, potentially up to 5, and extending the extrapolation to depths of 5 meters. Furthermore, expanding the scope of station inclusion to a global scale is recommended to ensure comprehensive coverage of all soil types.

The primary advantage of the qDTR methodology is its ability to yield higher average ratings throughout most of the year compared to the annual industry rating, resulting in an average increase of 7%. Moreover, it has the potential to further widen the disparity between winter and summer seasons, with an increase of up to 8.1%.

References

[1] H. Sugihara and T. Funaki, "Fundamental analysis of electrothermal coordination of underground cables toward high-penetration renewable generation," in *2018 IEEE Power Energy Society General Meeting (PESGM)*, 2018, pp. 1–5.

[2] B. J. van Ruijven, E. De Cian, and I. Sue Wing, "Amplification of future energy demand growth due to climate change," *Nature Communications*, vol. 10, no. 1, p. 2762, Jun. 2019. [Online]. Available: https://doi.org/10.1038/s41467-019-10399-3

[3] H. Brakelmann and G. Anders, "Ampacity reduction factors for cables crossing thermally unfavorable regions," *IEEE Power Engineering Review*, vol. 21, no. 7, pp. 67–67, 2001.

[4] O. Sungmin and R. Orth, "Global soil moisture data derived through machine learning trained with in-situ measurements," *Scientific Data*, vol. 8, no. 1, p. 170, 2021. [Online]. Available: https://doi.org/10.1038/s41597-021-00964-1

[5] J. Muñoz Sabater, "ERA5-Land hourly data from 1950 to present," Copernicus Climate Change Service (C3S) Climate Data Store (CDS), 2019, DOI: 10.24381/cds.e2161bac.

[6] Wang, P. and et al., "Dynamic thermal analysis for underground cables under continuously fluctuant load considering time-varying van wormer coefficient," *Electric Power Systems Research*, vol. 199, p. 107395, 2021. [Online]. Available: {https://doi.org/10.1016/j.epsr.2021.107395}

[7] M. Diaz-Aguiló and F. de León, "Introducing mutual heating effects in the ladder-type soil model for the dynamic thermal rating of underground cables," *IEEE Transactions on Power Delivery*, vol. 30, pp. 1958–1964, 2015.

[8] R. S. Olsen, G. J. Anders, J. Holboell, and U. S. Gudmundsdottir, "Modelling of dynamic transmission cable temperature considering soil-specific heat, thermal resistivity, and precipitation," *IEEE Transactions on Power Delivery*, vol. 28, pp. 1909–1917, 2013.

[9] P. Wang, H. Ma, G. Liu, Z. Han, D. Guo, T. Xu, and L. Kang, "Dynamic thermal analysis of high-voltage power cable insulation for cable dynamic thermal rating," *IEEE Access*, vol. 7, pp. 56 095–56 106, 2019.

[10] D. Douglass and A.-A. Edris, "Real-time monitoring and dynamic thermal rating of power transmission circuits," *IEEE Transactions on Power Delivery*, vol. 11, no. 3, pp. 1407–1418, 1996.

[11] G. Anders and M. El-Kady, "Transient ratings of buried power cables. i. historical perspective and mathematical model," *IEEE Transactions on Power Delivery*, vol. 7, no. 4, pp. 1724–1734, 1992.

[12] S. Karimi, P. Musilek, and A. M. Knight, "Dynamic thermal rating of transmission lines: A review," *Renewable and Sustainable Energy Reviews*, vol. 91, pp. 600–612, 2018. [Online]. Available: https://www.sciencedirect.com/science/article/pii/S1364032118302119

[13] K. Morozovska, "Dynamic rating with applications to renewable energy," Ph.D. dissertation, KTH, Electromagnetic Engineering, 2020, qC 20200109.

[14] W. Wang and S. Pinter, "Dynamic line rating systems for transmission lines: Topical report," *US Department of Energy, Office of Electricity Delivery & Energy Reliability*, 2014.

[15] S. Cherukupalli and G. J. Anders, *Types of Power Cables and Cable with Integrated Fibers*, 2019, pp. 77–93.

[16] D. Douglass, "Increased power flow through transmission circuits: Overhead line case studies and quasi-dynamic rating."

[17] *IEEE Guide for Thermal Resistivity Measurements of Soils and Backfill Materials*, Std., 2018.

[18] I. E. Commission, *Electric cables – Calculation of the current rating – Part 1-1: Current rating equations (100 % load factor) and calculation of losses – General*, IEC Standard 60 287-1-1, 2015.

[19] C. Kittel, H. Kroemer, and H. L. Scott, *Thermal Physics, 2nd ed.*, 1998, vol. 66.

[20] "Handbook of applied hydrology," V. T. Chow, D. R. Maidment, and L. W. Mays, Eds. New York, NY: McGraw-Hill Education, 1988.

[21] E. Dorison, G. J. Anders, and F. Lesur, "Ampacity calculations for deeply installed cables," *IEEE Transactions on Power Delivery*, vol. 25, no. 2, pp. 524–533, 2010.

[22] B. J. Cosby, G. M. Hornberger, R. B. Clapp, and T. R. Ginn, "A statistical exploration of the relationships of soil moisture characteristics to the physical properties of soils," *Water Resources Research*, vol. 20, no. 6, pp. 682–690, 1984. [Online]. Available: https://agupubs.onlinelibrary.wiley.com/doi/abs/10.1029/WR020i006p00682

[23] Dorigo, W. A. and et al., "The International Soil Moisture Network: a data hosting facility for global in situ soil moisture measurements," *Hydrology and Earth System Sciences*, vol. 15, pp. 1675–1698, 2011. [Online]. Available: {https://doi.org/10.5194/hess-15-1675-2011}

[24] A. Tavakol, K. R. McDonough, V. Rahmani, S. L. Hutchinson, and J. S. Hutchinson, "The soil moisture data bank: The ground-based, model-based, and satellite-based soil moisture data," *Remote Sensing Applications: Society and Environment*, vol. 24, p. 100649, 2021. [Online]. Available: https://www.sciencedirect.com/science/article/pii/S2352938521001853

[25] W. Dorigo, W. Wagner, C. Albergel, F. Albrecht, G. Balsamo, L. Brocca, D. Chung, M. Ertl, M. Forkel, A. Gruber, E. Haas, P. D. Hamer, M. Hirschi, J. Ikonen, R. de Jeu, R. Kidd, W. Lahoz, Y. Y. Liu, D. Miralles, T. Mistelbauer, N. Nicolai-Shaw, R. Parinussa, C. Pratola, C. Reimer, R. van der Schalie, S. I. Seneviratne, T. Smolander, and P. Lecomte, "Esa cci soil moisture for improved earth system understanding: State-of-the art and future directions," *Remote Sensing of Environment*, vol. 203, pp. 185–215, 2017, earth Observation of Essential Climate Variables. [Online]. Available: https://www.sciencedirect.com/science/article/pii/S0034425717303061

[26] G. Balsamo, P. Viterbo, A. Beljaars, B. van den Hurk, M. Hirschi, A. Betts, and K. Scipal, "A revised hydrology for the ecmwf model: Verification from field site to terrestrial water storage and impact in the integrated forecast system," p. 28, 04/2008 2008. [Online]. Available: https://www.ecmwf.int/node/7921

[27] S. O, E. Dutra, and R. Orth, "Robustness of process-based versus data-driven modeling in changing climatic conditions," *Journal of Hydrometeorology*, vol. 21, no. 9, pp. 1929 – 1944, 2020. [Online]. Available: https://journals.ametsoc.org/view/journals/hydr/21/9/jhmD200072.xml

[28] T. Hengl, J. Mendes de Jesus, G. Heuvelink, M. Ruiperez Gonzalez, M. Kilibarda, A. Blagotic, S. Wei, M. Wright, X. Geng, B. Bauer-Marschallinger, M. Guevara, R. Vargas, R. MacMillan, N. Batjes, J. Leenaars, E. Carvalho Ribeiro, I. Wheeler, S. Mantel, and B. Kempen, "Soilgrids250m: Global gridded soil information based on machine learning," *PLoS ONE*, vol. 12, no. 2, 2017.

[29] M. ElSaadani, E. Habib, A. M. Abdelhameed, and M. Bayoumi, "Assessment of a spatiotemporal deep learning approach for soil moisture prediction and filling the gaps in between soil moisture observations," *Frontiers in Artificial Intelligence*, vol. 4, 2021. [Online]. Available: https://www.frontiersin.org/articles/10.3389/frai.2021.636234

[30] M. Taheri, H. K. Schreiner, A. Mohammadian, H. Shirkhani, P. Payeur, H. Imanian, and J. H. Cobo, "A review of machine learning approaches to soil temperature estimation," *Sustainability*, vol. 15, no. 9, 2023. [Online]. Available: https://www.mdpi.com/2071-1050/15/9/7677

[31] Delbari, M. and Sharifazari, S. and Mohammadi, E., "Modeling daily soil temperature over diverse climate conditions in Iran—a comparison of multiple linear regression and support vector regression techniques," *Theoretical and Applied Climatology*, vol. 135, pp. 991–1001, 2019. [Online]. Available: {https://doi.org/10.1007/s00704-018-2370-3}

[32] A. Rani, N. Kumar, J. Kumar, J. Kumar, and N. K. Sinha, "Chapter 6 - machine learning for soil moisture assessment," in *Deep Learning for Sustainable Agriculture*, ser. Cognitive Data Science in Sustainable Computing, R. C. Poonia, V. Singh, and S. R. Nayak, Eds. Academic Press, 2022, pp. 143–168. [Online]. Available: https://www.sciencedirect.com/science/article/pii/B978032385214200001X

[33] R. Huang, J. A. Pilgrim, P. L. Lewin, D. Scott, and D. Morrice, "Use of day-ahead load forecasting for predicted cable rating," in *IEEE PES Innovative Smart Grid Technologies, Europe*, 2014, pp. 1–6.

[34] R. Huang, J. A. Pilgrim, P. L. Lewin, and D. Payne, "Dynamic cable ratings for smarter grids," in *IEEE PES ISGT Europe 2013*, 2013, pp. 1–5.

[35] A. Bracale, P. Caramia, P. De Falco, A. Michiorri, and A. Russo, "Day-ahead and intraday forecasts of the dynamic line rating for buried cables," *IEEE Access*, vol. 7, pp. 4709–4725, 2019.

[36] Campbell, G. S., *Soil Physics with BASIC: Transport Models for Soil-Plant Systems*, 1st ed., November 1 1985, vol. 14.

[37] DeVries, D. A., "Thermal Properties of Soils," in *Physics of Plant Environment*, W.R. van Wijk, Ed. Amsterdam: North-Holland Publishing Company, 1963.

[38] He, H. and Zhao, Y. and Dyck, M. F. and et al., "A modified normalized model for predicting effective soil thermal conductivity," *Acta Geotechnica*, vol. 12, pp. 1281–1300, 2017, Received: 30 November 2016, Accepted: 02 May 2017, Published: 10 June 2017, Issue Date: December 2017. [Online]. Available: {https://doi.org/10.1007/s11440-017-0563-z}

[39] Xiong, K. and Feng, Y. and Jin, H. and et al., "A new model to predict soil thermal conductivity," *Scientific Reports*, vol. 13, p. 10684, 2023, Received: 27 March 2023, Accepted: 21 June 2023, Published: 01 July 2023. [Online]. Available: {https://doi.org/10.1038/s41598-023-37413-5}

[40] Lu, Y. and Lu, S. and Horton, R. and Ren, T., "An Empirical Model for Estimating Soil Thermal Conductivity from Texture, Water Content, and Bulk Density," *Soil Science Society of America Journal*, vol. 78, pp. 1859–1868, 2014. [Online]. Available: {https://doi.org/10.2136/sssaj2014.05.0218}

[41] O. Johansen, "Thermal conductivity of soils," p. 322, 07 1977.

[42] Ren, J. and Men, L. and Zhang, W. and et al., "A new empirical model for the estimation of soil thermal conductivity," *Environmental Earth Sciences*, vol. 78, p. 361, 2019, Received: 13 August 2018, Accepted: 01 June 2019, Published: 11 June 2019. [Online]. Available: {https://doi.org/10.1007/s12665-019-8360-7}

[43] W. Dorigo, I. Himmelbauer, D. Aberer, L. Schremmer, I. Petrakovic, L. Zappa, W. Preimesberger, A. Xaver, F. Annor, J. Ardö *et al.*, "The international soil moisture network: serving earth system science for over a decade," *Hydrology and earth system sciences*, vol. 25, no. 11, pp. 5749–5804, 2021.

[44] R. Hiederer, "Mapping Soil Properties for Europe - Spatial Representation of Soil Database Attributes," Publications Office of the European Union, Luxembourg, EUR 26082EN, 2013.

[45] Copernicus Climate Change Service, "Climate and energy indicators for Europe from 2005 to 2100 derived from climate projections," Copernicus Climate Change Service (C3S) Climate Data Store (CDS), 2021, DOI: 10.24381/cds.f6951a62.

[46] Montana Salas, Sergio Daniel and Michiorri, Andrea, "Weather-Based Quasi Dynamic Thermal Ratings for Power Transformers," in *IEEE PES ISGT Europe 2023*, Grenoble, France, October 2023. [Online]. Available: {https://hal.archives-ouvertes.fr/hal-04227016v2}

[47] Hadiwidjaja, Stella and Montana Salas, Sergio Daniel and Michiorri, Andrea, "Quasi-Dynamic Line Rating spatial and temporal analysis for network planning," 2023. [Online]. Available: {https://hal.archives-ouvertes.fr/hal-03766110v2}

[48] W. Dorigo, A. Xaver, M. Vreugdenhil, A. Gruber, A. Dostálová, A. D. Sanchis-Dufau, D. Zamojski, C. Cordes, W. Wagner, and M. Drusch, "Global automated quality control of in situ soil moisture data from the international soil moisture network," *Vadose Zone Journal*, vol. 12, no. 3, p. vzj2012.0097, 2013.

[49] F. Pedregosa, G. Varoquaux, A. Gramfort, V. Michel, B. Thirion, O. Grisel, M. Blondel, P. Prettenhofer, R. Weiss, V. Dubourg, J. Vanderplas, A. Passos, D. Cournapeau, M. Brucher, M. Perrot, and E. Duchesnay, "Scikit-learn: Machine learning in Python," *Journal of Machine Learning Research*, vol. 12, pp. 2825–2830, 2011.

[50] "Soil Taxonomy: A Basic System of Soil Classification for Making and Interpreting Soil Surveys," 1999.

[51] LeCun, Y. and Bengio, Y. and Hinton, G., "Deep learning," *Nature*, vol. 521, pp. 436–444, 2015, Received: 25 February 2015, Accepted: 01 May 2015, Published: 27 May 2015, Issue Date: 28 May 2015. [Online]. Available: {https://doi.org/10.1038/nature14539}

[52] T. Chen and C. Guestrin, "XGBoost: A scalable tree boosting system," in *Proceedings of the 22nd ACM SIGKDD International Conference on Knowledge Discovery and Data Mining*, ser. KDD '16. New York, NY, USA: ACM, 2016, pp. 785–794. [Online]. Available: http://doi.acm.org/10.1145/2939672.2939785

[53] L. Breiman, "Random forests," *Machine learning*, vol. 45, pp. 5–32, 2001.

[54] R. Tibshirani, "Regression Shrinkage and Selection Via the Lasso," *Journal of the Royal Statistical Society: Series B (Methodological)*, vol. 58, no. 1, pp. 267–288, Dec. 2018, _eprint: https://academic.oup.com/jrsssb/article-pdf/58/1/267/49098631/jrsssb_58_1_267.pdf. [Online]. Available: https://doi.org/10.1111/j.2517-6161.1996.tb02080.x

[55] S. Seabold and J. Perktold, "statsmodels: Econometric and statistical modeling with python," in *9th Python in Science Conference*, 2010.

[56] T. Akiba, S. Sano, T. Yanase, T. Ohta, and M. Koyama, "Optuna: A next-generation hyperparameter optimization framework," in *Proceedings of the 25th ACM SIGKDD International Conference on Knowledge Discovery and Data Mining*, 2019.

[57] R. Hiederer, "Mapping Soil Properties for Europe - Spatial Representation of Soil Database Attributes," Publications Office of the European Union, Luxembourg, Tech. Rep. EUR26082EN, 2013.

[58] A. Clauset, C. R. Shalizi, and M. E. J. Newman, "Power-law distributions in empirical data," *SIAM Review*, vol. 51, no. 4, p. 661–703, Nov. 2009. [Online]. Available: http://dx.doi.org/10.1137/070710111

[59] T.-F. K. S.A., *High and extra high voltage cables*, edition ed. City: www.tfkable.com, 2019, https://www.tfkable.com/en_pl/catalogs-and-brochures/catalogues.html.

[60] Eurostat, "Statistical regions in the european union and partner countries — nuts and statistical regions 2021," European Union, Tech. Rep., 2021, product code: KS-GQ-20-092, ISBN 978-92-76-10625-8, ISSN 2315-0815.

[61] T. Brown, D. Schlachtberger, A. Kies, S. Schramm, and M. Greiner, "PyPSA-Eur: An open optimisation model of the european electricity system," *Zenodo*, 2020. [Online]. Available: https://doi.org/10.5281/zenodo.3602442

[62] S.-D. Montana and A. Michiorri, "The climate change impact on power grid transmission capacity," 2024, submited.